

A PROPORTIONAL CHAMBER SYSTEM
FOR THE SLAC 20-GeV SPECTROMETER*

E. Bloom, R. L. A. Cottrell, G. Johnson,
C. Prescott, R. Siemann, and S. Stein
Stanford Linear Accelerator Center
Stanford University, Stanford, California 94305

ABSTRACT

A 400-wire proportional chamber system has been used in two electron scattering experiments with the SLAC 20-GeV spectrometer. Chamber construction and associated electronics are described in detail, and the resultant performance during data taking (over a three-month period) is discussed.

(Submitted to Nucl. Instr. and Methods)

* Work supported by the U. S. Atomic Energy Commission.

INTRODUCTION

Before October 1970, a scintillation-counter hodoscope system was used in most experiments with the SLAC 20-GeV spectrometer.¹ This system had several disadvantages, some inherent with scintillation hodoscopes and some peculiar to the design for the 20-GeV spectrometer. These disadvantages are detailed below.

The hodoscope system consisted of four hodoscopes with average thicknesses of (in the order traversed by a particle) 1.0 gm/cm^2 , 1.0 gm/cm^2 , 2.0 gm/cm^2 and 4.0 gm/cm^2 . The large amount of material in these hodoscopes made the probability for secondary electron production large. Typically, the momentum or scattering angle could not be determined because of uninterpretable hodoscope patterns for 8% of the events identified as electrons (in electron scattering experiments).

The bin size and efficiency of the hodoscope elements were not uniform at the 10% level. Statistically significant structure in a momentum or scattering angle distribution could arise from this nonuniformity. The technique of scanning developed by A. Boyarski² can be used to minimize the effect of this nonuniformity in the momentum (but not the scattering angle) distribution.

The last two hodoscopes were located at the scattering angle and momentum foci of the spectrometer, and they were sufficient if one had no contamination from backgrounds such as scattering from magnet pole faces. If additional information was needed to reject background, all four hodoscopes had to be used. The disadvantage of adding the first two hodoscopes was the introduction of more material into the detector. With the four hodoscopes, one still did not have any redundancy in the measurement of a trajectory. The lack of space and the desire to add no more mass to the detector prevented the use of additional hodoscopes.

The data-taking rate was limited because the hodoscope electronics could process only one event per SLAC beam pulse (1.6 μ sec long). The use of a missing mass hodoscope³ was a solution to this problem at the expense of losing hodoscope information on an event-by-event basis.

The work of Charpak et al.,⁴ indicated that multiwire proportional chambers would be a solution to the hodoscope mass and bin size nonuniformity problems. Because of the small mass, a fifth chamber could be added to the basic system of four chambers; this would permit redundancy in the vertical trajectory measurement. A five-plane proportional chamber system complete with associated electronics was designed as a replacement for the hodoscopes. To allow an increase in data rate, the electronics were designed to process four events per SLAC pulse.

This system has been successfully used in two electron scattering experiments⁵ at SLAC. The design, construction and details of the performance of this system are described in this paper.

PROPORTIONAL CHAMBER CONSTRUCTION

All five chambers were identical; top and side views are shown in Fig. 1.

A. Design Considerations

An ionizing particle passing through the chamber leaves a track of ion-electron pairs from high voltage (HV) plane to HV plane. The electrons drift to the proportional wires at a typical speed of 5×10^6 cm/sec (200 nsec/cm).⁶ The electrons produced far from the proportional wires do not contribute useful information about the track location. Figure 2 shows the efficiency of a chamber as a function of the delay added to a scintillation counter trigger before it is put in coincidence with the wires. The word efficiency as used in this paper

means

$$\text{efficiency} = \frac{\text{Number of events with one or more wires in coincidence with the scintillation counter trigger}}{\text{Number of events with a scintillation counter trigger}}$$

In Fig. 2 the peak value of the efficiency is $98.7 \pm 0.4\%$, and the delay curve has a 90-nsec-long tail where the efficiency is approximately constant at 11%. This tail is produced by events which have counted on at least two wires, one when the efficiency of the chamber is almost 100% and the other at a later time. The length of the tail is consistent with the drift time for the 4-mm gap from HV plane to proportional wire (PW) plane. The gain of the avalanche in the chamber is sufficient to give a detectable signal from only one or two electron-ion pairs; electron-ion pairs produced far from the center of the chamber are not needed to detect a particle. These pairs are not needed for locating a track, but they contribute to the dead time and memory time of the chamber. By narrowing the HV to PW spacing one eliminates these pairs and decreases the dead time and memory time. However, to allow reasonable working tolerances, a 4-mm HV to PW separation was chosen.

The momentum dispersion of the 20-GeV spectrometer is 0.303%/cm, and the momentum resolution is $\pm 0.05\%$. The corresponding numbers for the scattering angle dispersion and resolution are 0.640 milliradian/cm and ± 0.1 milliradian. Bin sizes smaller than 2.8 mm would not significantly improve the spectrometer resolution. In our application the advantages of closer (than 2.8 mm) wire spacing were a decrease in the chamber jitter time and better background rejection associated with the improved trajectory determination. The reliability and ease of operation of chambers with 2-mm wire spacing compared to those with 1-mm spacing were the dominant factors in the choice of 2-mm spacing.

B. Materials and Assembly

The chambers were constructed in two halves which were clamped together with an O-ring providing the gas seal. The two halves were identical except that on one half the wire frame was replaced by a 1.59-mm-thick copper-clad epoxy board. The wire frame will be discussed in more detail later.

First consider the common features of the two halves. The operating pressure of the chambers was only slightly above atmospheric,⁷ so 76-micron-thick mylar was used for the windows. An aluminum-nylon cloth (consisting of 0.25-mm-diameter aluminum wires spaced 1 mm apart with 0.25-mm-diameter nylon wire woven around these aluminum wires) was used for the HV plane. A screen was desirable for the HV plane because it allowed one to look into the chamber for visual inspection and simplified problems of gas flow; the aluminum-nylon cloth was chosen because of its low mass and availability.

The spacers were made from epoxy board (G10) or copper-clad epoxy board (G10) as indicated in Fig. 1. Each spacer was made from a single piece of epoxy board with the active area of chamber cut out of the center; grooves were cut close to the active area to prevent epoxy entering the chamber during assembly. Stycast 1266 (Ref. 8) was used to join the components of the chamber half, and Silverprint⁹ formed the electrical contact between the HV spacer and HV plane. The first step in building the chamber was the assembly of the halves. All components were thoroughly cleaned before and after this assembly; throughout assembly of the chambers extreme care was taken to insure that grease, epoxy, lint or other dirt did not get into the active area of the chamber.

The proportional wires were a smooth grade of gold-coated tungsten with a 20-micron diameter.¹⁰ Although considerably smoother than the normal grade of wire, when examined under a microscope this wire was seen to have

considerable scoring from the die through which it was drawn (see Fig. 1d). Although this imperfection of the wire did not affect the performance of the chambers described in this paper, it may have been one source of the difficulties in obtaining reliable chambers with 1-mm wire spacing. The wire was wound onto a large (50 cm square by 2.5 cm high) metal frame by a mechanism employing an eddy current feedback device to keep a constant tension of $5.4 \pm 0.1 \times 10^4$ dynes. The ends of the frame were grooved to accurately space the wire; the random deviation from the 2-mm wire spacing was less than ± 50 microns (or $\pm 2.5\%$ of the bin size).

Once the frame was wound, the chamber half with the wire frame was placed beneath the wires, aligned with respect to them, and then raised until it just touched the wires. With the large frame still holding the tension on the wires, they were epoxied to the wire frame. Larger diameter wires (30, 76, and 152 microns, respectively) were placed between the 20-micron diameter wires and the edge of the aperture as shown in Fig. 1a; these prevented excessive field gradients on the wires at the edge of the active area. The completed chambers had 94 active wires.

The wire frame was actually a large printed circuit card; it served to make the connection from the proportional wires to the electronics. Eight wires were connected to a 22-pin circuit card connector¹¹ (see Fig. 1c).

To prevent cross talk between wires, the trace lengths on the wire frame were kept as short as practical, and each wire was isolated from its nearest neighbor at the connector by a pin connected to ground. Once the wires were epoxied to the wire frame, they were cut and soldered to the wire frame using a controlled soldering iron temperature and low-melting temperature solder to avoid evaporating the gold plating.

After final checks of wire tension and electrical contact, the connectors were placed in the wire frame, alignment mounts were attached and measured relative to the center of the chamber with an accuracy of ± 50 microns, and the two halves were clamped together with a 0.49-mm-diameter soft O-ring¹² sealing the chamber. Thin (125 microns) opaque polyethylene sheets were taped over the windows to prevent photoelectrons caused by the room lights shining on the aluminum HV screen. Figures 3 and 4 show two views of a completed chamber.

ELECTRONICS

We wish to discuss the electronics with an emphasis on the interaction with the chamber system; an alternate description of the electronics is available.¹³

A. Design Considerations

Figure 5 shows a block diagram for the high-speed electronics. All the electronics except the amplifier and cable driver were remote from the chamber. This choice was made because of the availability of the necessary 50Ω cables and the desire for easy access to as much of the electronics as practical (the chambers were located in a controlled-access radiation area). These cables were longer than the cables of the trigger electronics by a sufficient amount so that no additional delay was needed in the proportional chamber signals.

Each wire was placed in coincidence with four gate signals. Thus, up to four events per SLAC beam pulse could be processed, and data could be taken at an average rate of one event per SLAC pulse without appreciable data loss. Cost considerations and available integrated circuits led to the choice of parallel event gates, coincidence gates, latches and readout gates.

We chose to use the MECL II (Ref. 14) family of integrated circuits to have electronics with resolving times smaller than the 30-nsec jitter time of the chamber.

B. Amplifier

The amplifier was an MC1035 wired as a cascaded triple differential amplifier with bias feedback. The amplifier output drove 670 nsec of high quality 50 Ω cable (90 nsec of RG58c/u and 580 nsec of Amphenol Foam 8) through a two-transistor cable driver; the circuit diagram for the amplifier and cable driver is shown in Fig. 6. The amplifier had a nominal gain of 600, was sensitive to 300 microvolt input pulses, and the output limited at -700 mV. The gain and sensitivity figures are typical; there were channel-to-channel variations in these numbers.

Experience taught us that these channel-to-channel variations were not important. The gain of the proportional multiplication in the chamber was sufficient to produce amplifier outputs that were limited for minimum ionizing particles with a gas mixture of 20% isobutane and 80% argon used throughout. Typical signals (before being attenuated by the cable) from minimum ionizing particles were -700 mV in amplitude and 600-800 nsec long. The risetime of these signals was consistent with the amplifier risetime (7-10 nsec).

We did not have a pulse shaper at the chamber because pulse length information was useful in diagnosing problems with the chamber performance. Pulses significantly longer than 800 nsec were indications of potential breakdown in the chamber.

The amplifiers were packaged in cards of eight which mated with the sockets mounted in the wire frame of the chamber. Considerable care was necessary to avoid oscillations and cross talk between amplifiers; this was done through the extensive use of ground planes to decouple amplifier channels and avoid ground currents. Both the power and ground for the amplifiers was supplied through the wire frame, and the isolation between wires established on the wire frame

was maintained on the amplifier card (see Fig. 1c and 7). The resultant circuit card is shown in Fig. 7; detailed information on this layout is available on request.

C. Latch Circuit

The circuit diagram for a single channel of the latch circuit is shown in Fig. 8; this circuit contained discrimination, coincidence and storage elements.

The first stage was an MC1035 wired as a line receiver, discriminator and pulse shaper. To avoid ground loops, the high-voltage cable provided the only ground for the chamber; the line receiver allowed the amplifier signal to be introduced into the latch without locally grounding the shield of the cable. The discriminator was a Schmidt trigger with a -300 mV threshold. The -700 mV amplitude, 7 nsec risetime amplifier signal was distorted by the 670 nsec cable. The leading edge of the pulse was approximately linear from -70 mV to -400 mV (15 nsec was the typical time to make this transition); the distortion was significant above -400 mV amplitude. Therefore, the -300 mV threshold was low enough to prevent time-slewing, but still gave good noise immunity.

The output of the Schmidt trigger was differentiated and then shaped by the final stage of the MC1035. The output of the pulse shaper was an 8-nsec-wide MECL level pulse with timing determined by the leading edge of the amplifier signal.

A coincidence was then formed with four different event-gate signals in a single MC1010, and the coincidence gate outputs were stored in latches made from MC1010's. In our experiments the four event gates were a time-ordered sequence of indications of the passage of electrons through the apparatus. For the remainder of this paper we define the event levels as these time-ordered indications; for example, the third event level corresponds to the third electron which passed through the apparatus during a beam pulse.

The latch circuits were packaged in single-width CAMAC modules with eight wires per module. Sixteen such modules plus gate fanout circuits and a crate controller filled a CAMAC crate. The system occupied a total of four CAMAC crates.

D. Data-Handling Electronics

The readout used a specially designed CAMAC crate controller and was based on the use of the CAMAC branch highway.

A scanner searched for and read the (12 bit) address of each set latch. An SDS-9300 computer was interrupted after each pair of addresses was read, and the resultant 24-bit word transferred to the computer. After interrogating all the latches, the scanner sent the computer the number of set latches which could be compared with the number initially read by the computer. The scanner then reset the latches and signalled the computer that the data transfer was completed. This operation occurred after each beam pulse with at least one trigger and was completed before the next beam pulse arrived.

CHAMBER PERFORMANCE

Figure 9 shows the detector scheme of the 20-GeV spectrometer. The proportional chambers are denoted by X1, X2, Y1, Y2 and Y3. The X chambers measured the scattering angle (the horizontal coordinate), and the Y chambers measured the momentum (the vertical coordinate). All trajectories were approximately perpendicular to the chambers. The event trigger was a coincidence between either one of the two phototubes on scintillation counter TR3 and the total absorption counter TA. The timing of the trigger was determined within ± 2 nsec of the passage of a particle by TR3, and the TA bias was such that the counter was 99% efficient for electrons with energy greater than (or equal to) 2.5 GeV. The proportional-chamber gate was a 34 nsec wide pulse with timing

determined by the event trigger. All trajectories within the solid angle and momentum acceptance defined by a TR1-TR3 coincidence passed through the active area of all five chambers. By studying events with TR1-TR3 coincidence we had a continuous measure of the chamber efficiency. Counter TR2 defined a restricted solid angle, and the dE/dx and CT counters were used for particle identification. None of these latter counters was directly related to the proportional chambers. Figure 10 is a photograph of the detector.

Before installation in the spectrometer each chamber was tested with a Bi²⁰⁷ source. In addition, the optimum high voltage was determined and the efficiency measured for each chamber in a secondary beam (5 to 15 GeV π^- 's) at SLAC. We observed that the jitter time of the chambers decreased as the high voltage increased; therefore the maximum high voltage with no evidence of sparking (as determined by the output pulse length) was used. All five chambers had an operating high voltage between 2750 and 2850 volts.

After installation in the spectrometer the chambers, electronics and cables were checked by using the Bi²⁰⁷ source and by simultaneously pulsing all the wires. The latter test was done by applying a five-volt pulse to the high voltage screen (through a capacitive coupling), and looking at the signal picked up on each wire.

A delay curve was taken for each wire to be sure that the total delay to the coincidence gates was the same for each wire. This was done simultaneously for all wires by having the computer accumulate and display a two-dimensional array $P(i, j)$ where i is the number of the wire, j indicates the value of the delay put into the event-gate signal (before it is fanned out), and P is the probability (per event gate) of a coincidence between wire i and the event gate. The delays of wires with delay curves centered more than ± 4 nsec from the mean were

compensated by adding or removing cable. It was necessary to adjust the delay of 6 wires out of 400. These delay adjustments were necessary because of slight differences in the propagation delay of the electronics and different length cable routes. The variation in delay from wire to wire did not originate in the chamber. In fact, each chamber had the same delay at its operating high voltage. This identical performance of the chambers made it possible to interchange and replace chambers with ease. Once the necessary adjustments of the individual delays were made, a final delay curve was taken with a TR1-TR3-TA coincidence as the event gate. Figure 11 shows the Y2 delay curve; all chambers had similar delay curves. It was checked that all four event levels had peaks in their delay curves at the same value of delay; the final trigger delay was set to this value.

Numerous subroutines were written to monitor the performance of the chambers on-line. These included routines related directly to the performance of an individual chamber, routines which monitored the efficiency of track reconstruction, and routines which histogrammed the resultant intercepts and slopes of the trajectory. An event was analyzed by these routines if there was an indication that the particle had gone through counter TR1 and was identified as an electron on the basis of the TA pulse height.

The "number of wires per event" subroutine histogrammed the number of times a trigger would be accompanied by 0, 1, 2, ... wires in each plane. This information was compiled separately for each plane and for each of the first three event levels, and it showed the deadtime effects for the second and third levels (recall that the second (third) level consisted of events which were the second (third) event trigger in a SLAC beam pulse). Figure 12 shows this distribution for a typical run and chamber Y2. As this figure shows, typically 8% of the first-level events had zero or more than one wire per event. The chamber

deadtime is shown by the increase in the probability of zero wires per event with levels two and three. Table I is a summary of the percentage of events with zero wires for an entire experiment (4134 runs and 2.8×10^7 events). The deadtime effect was consistent with a 600-800-nsec deadtime per wire (the deadtime was approximately equal to the amplifier pulse length) and an average of 1.2 wires counting per event.

The SLAC 20-GeV spectrometer disperses momentum in the vertical plane. The vertical component of a trajectory can have a considerable range of slopes in the detector (typically 22.6 milliradians full width) because the vertical projected angle at the target and the momentum both contribute significantly to the vertical trajectory. The scattering angle (the horizontal projected angle of an event at the target) is measured by parallel-to-point focusing in the horizontal plane. All horizontal trajectories are approximately parallel in the detector; the typical distribution has a full width of 2 milliradians.

The small width of the horizontal-slope distribution makes a third X chamber unnecessary. For the small percentage of events (1.8% of all events) when either X1 or X2 failed, the scattering angle of the event could be determined from the other chamber. If X2 failed there was no loss in resolution because X1 was at the scattering angle focus of the spectrometer, and if X1 failed one made an error of ± 0.12 milliradian (± 1.9 mm in the intercept at the focus) in the scattering angle. This latter error is comparable to the spectrometer resolution. When redundancy was needed to resolve the trajectory position at the scattering angle focus, the two X chambers were sufficient because of the narrow distribution in the horizontal slope.

The broad distribution of possible vertical trajectory slopes made three Y chambers necessary to achieve efficiency and redundancy. If one had a two

chamber system with one chamber at the momentum focus (Y2), then the second chamber gives no useful information if Y2 fails. In this case the error in the position of the trajectory at Y2 is approximately ± 1.3 cm ($\pm 0.4\%$ in momentum) which is much greater than the spectrometer resolution. Similarly, two Y chambers could not resolve those ambiguous events with wires closer than 2.5 cm having counted.

The track-fitting procedure used the philosophy outlined above. Wires were first grouped; for each plane all contiguous wires (up to 5) were classified as a group (two groups of one or two wires separated by one wire which did not count were treated as a single larger group) and the center coordinate and bin size of the group was determined. If a plane contained a group of more than five wires or more than 4 groups, that chamber was ignored in further analysis of the event. The number of groups per plane and per event was constantly monitored on-line as a check of the performance of the chambers. Most events had one group in each plane. Table II shows the distribution of different types of groups for a typical run. Figure 13 shows the distribution of events with one group in each chamber for 2.8×10^7 events; for the first event level 92% of the events had a single group in each X chamber and 89% of the events had a single group in each Y chamber. The average trigger rate at which these data were taken was 500 kHz and the singles rate in the chamber ranged from one to three times the trigger rate.

For an event to have a good track in the horizontal dimension it was necessary to obtain an unambiguous measurement of the intercept at the scattering angle focus. Using the redundancy provided by the two X chambers it was possible to reconstruct a single track in the horizontal dimension in typically 98% of the first-level events. Almost all of the remaining 2% of the events had two tracks

in the horizontal dimension. The percentage of events with a single horizontal track in the second and third event levels were 97% and 96%, respectively. Table III gives a more detailed summary of the track reconstruction efficiency for a typical run.

In the vertical track reconstruction, it was necessary to get an unambiguous measurement of the slope and intercept to have a good track. This was possible in typically 98% of the first-level events, 97% of the second-level events and 95% of the third-level events. Approximately half the inefficiency was due to events with two vertical tracks, and half was due to events with no vertical tracks. See Table III for more details.

Figure 14 shows the track reconstruction efficiency for 2.8×10^7 events. The percentage of events with a single track in both dimensions are $95.8 \pm 1.0\%$, $93.3 \pm 1.5\%$ and $90.8 \pm 2\%$ for the three event levels. The chambers lose an average of 2.5% efficiency per event level.

These data show that when deadtime and memorytime problems were not serious (event level 1) the track reconstruction efficiency was high, and by building a system with a minimal amount of redundancy it was possible to take high-quality data even on the third event in a beam pulse (corresponding to instantaneous rates of approximately 2 MHz).

One of the desirable features of proportional chambers was the uniformity of the bin-to-bin efficiency. The construction technique and subsequent measurements indicated that this uniformity would be present at the $\pm 2.5\%$ level. Figure 15a shows the distribution of events in chamber Y2 summed over several runs with high statistics; the statistical accuracy of a single bin in this distribution is $\pm 0.6\%$. A linear fit has been made to these data over the flat region of the distribution (from wire 20 to wire 70 as indicated in Fig. 15a). To obtain

a reasonable fit to these data it is necessary to add a $\pm 1.2\%$ random variation presumably from the bin-to-bin efficiency (making the total standard deviation 1.3%). The resultant deviations from the best linear fit are shown in Fig. 15b. The deviation of wire 32 from the fit is statistically significant. It is $4.5 \pm 1.3\%$ and is an indication that deviations from uniformity as large as 5% may exist. Analysis of the performance of the other chambers indicates that this deviation is the largest observed.

The chamber system was used for a total of 9 weeks of data taking over a four-month period. The estimated total number of particles through the chambers was $1-2 \times 10^8$. The distributions in Table I and Figs. 13 and 14 came from the last third of the running. No gradual deterioration of the performance of the chambers as a function of time was observed. During this time there was only one significant deviation from the performance described in this paper. One chamber arced from high voltage to proportional wires during the second week of running. Examination of the destroyed chamber showed that the cause of failure was a poor epoxy bond between the wire frame and proportional wires. The reliable performance of all the other chambers has convinced us that this failure was a fluke. Having an available replacement (which performed identically to the chamber which failed) allowed us to recover in a few hours.

CONCLUSIONS

We have described the components and resultant performance of a small proportional-chamber system of 400 wires. The low mass of the chambers and the redundancy in the system have led to a significant increase (compared to the previous hodoscopes) in the fraction of events with good trajectory information. With a redundant system the large deadtime per wire and the memory time of the chamber do not present significant problems at our data-taking rate of 0.5 to 2.0 MHz.

The chambers are significantly more uniform in bin size and efficiency than the hodoscope system. The average variation in the product of bin size and efficiency is $\pm 1.2\%$, but deviations as large as 5% may exist. The improvement in uniformity follows directly from the ease of construction and the low mass of proportional chambers.

Like most apparatus, many features of this system are peculiar to our physics interests and detection problems. However, the performance, ease of operation and reliability of this system show that proportional chambers should be given serious consideration as alternatives to scintillation hodoscopes.

Acknowledgements

Many people have made significant contributions to this proportional chamber system. We would particularly like to thank W. Atwood, M. Browne, K. Doty, R. Haley, D. Horelick, R. S. Larsen, J-L. Pellegrin, H. Piel, R. Taylor and W. Weeks.

FOOTNOTES AND REFERENCES

1. W.K.H. Panofsky, "Magnetic Spectrometers," Review talk presented at the High Energy Physics Instrumentation Conf., Sept. 8-12, 1970, Dubna, USSR (also Report No. SLAC-PUB-798, Sept. 1970).
2. A. Boyarski, R. Diebold, S. D. Ecklund, G. E. Fischer, Y. Murata, B. Richter and M. Sands, Phys. Rev. Letters 25, 695 (1970).
3. S. Rock, M. Borghini, O. Chamberlain, R. Fuzesy, C. Morehouse, T. Powell, G. Shapiro, H. Weisberg, R.L.A. Cottrell, J. Litt, L. Mo and R. Taylor, Phys. Rev. Letters 24, 748 (1970).
4. G. Charpak, R. Boucher, T. Bressani, J. Favier and C. Zupancic, Nucl. Instr. Methods 62, 262 (1968).
5. E. D. Bloom, R.L.A. Cottrell, H. DeStaebler, C. L. Jordan, H. G. Piel, C. Prescott, R. Siemann, S. Stein and R. E. Taylor, "Progress Report on Inelastic Electron Scattering at 4^0 ," submitted to the 1971 International Symposium on Electron and Photon Interactions at High Energies; and E. D. Bloom, R.L.A. Cottrell, H. DeStaebler, C. L. Jordan, G. Miller, H. Piel, C. Prescott, R. Siemann, C. K. Sinclair, S. Stein and R. E. Taylor, "Coincidence Electroproduction in the Region of the Rho Meson," 1971 International Symposium on Electron and Photon Interactions at High Energies, Cornell University, Ithaca, New York, August 23-27, 1971 (also Report No. SLAC-PUB-955, Aug. 1971).
6. W. N. English and G. C. Hanna, Can. J. Phys. 31, 768 (1953).
7. The chambers were operated at a pressure of 5 mm of silicon oil above atmospheric.
8. Emerson and Cuming, Inc., Gardena, California.
9. G. C. Electronics, Rockford, Illinois.

10. Grade EE 5% Au coated tungsten, Thermionic Products Company, Inc., Plainfield, New Jersey.
11. Connector model 2VH22/1AV5 manufactured by Viking Industries, Chatsworth, California.
12. 3/64-inch diameter silicon rubber, 30-durometer hardness.
13. B. Bertolucci, R. Carman, J. Faust, D. Horelick and J-L. Pellegrin, paper presented at the IEEE 1970 Nuclear Science Symposium, New York City, November 4-6, 1970 (also Report No. SLAC-PUB-836, Nov. 1970).
14. Motorola Semiconductor Products, Inc.

TABLE I
Percentage of Events with Zero Wires

Event Level	<u>Chamber</u>				
	Y1	Y2	Y3	X1	X2
1	1.1 (0.8)	0.35 (0.6)	0.35 (0.6)	0.4 (0.5)	0.3 (0.2)
2	3.8 (1.4)	2.0 (1.2)	1.8 (1.2)	2.0 (1.2)	1.8 (1.0)
3	5.2 (2.5)	3.8 (2.0)	3.6 (2.0)	3.8 (2.0)	3.5 (2.0)
1-3 (All Events)	2.0	0.9	0.9	1.0	0.8

A summary of the percentage of events with zero wires. This is a summary of the behavior during one experiment extending over one month (a total of 2.8×10^7 events). The percentage is the mean value of the distribution and the number in parentheses is the FWHM of the distribution.

TABLE II

The Fraction of Events with Different Groups for a Typical Run

Event Description	<u>X Planes</u>		
	Event Level 1	Event Level 2	Event Level 3
0 Groups in Both Planes	0.0001 ±0.0001	0.009 ±0.002	0.0 ±0.01
1 Group in One Plane and 0 Groups in the Other	0.0066 ±0.0007	0.021 ±0.004	0.03 ±0.02
1 Group in Both Planes	0.932 ±0.002	0.885 ±0.008	0.90 ±0.03
More than 1 Group in One Plane and 0 Groups in the Other	0.0006 ±0.0002	0.0006 ±0.0006	0.0 ±0.01
1 Group in One Plane and more than 1 in the other	0.051 ±0.002	0.070 ±0.007	0.05 ±0.01
More than 1 Group in each Plane	0.010 ±0.001	0.008 ±0.002	0.02 ±0.01
	<u>Y Planes</u>		
0 Groups in at least 2 Planes	0.0031 ±0.0004	0.005 ±0.002	0.02 ±0.01
1 Group in 2 Planes and 0 Groups in the third	0.014 ±0.001	0.051 ±0.006	0.07 ±0.03
1 Group in 3 Planes	0.886 ±0.003	0.83 ±0.01	0.79 ±0.05
0 Groups in 1 Plane More than one Group in a second Plane 1 or more Groups in a third Plane	0.0011 ±0.0003	0.005 ±0.002	0.02 ±0.01
One Group in 2 Planes and more than 1 Group in the third	0.079 ±0.002	0.095 ±0.008	0.08 ±0.03
More than one Group in two Planes	0.015 ±0.001	0.012 ±0.003	0.02 ±0.01

TABLE III

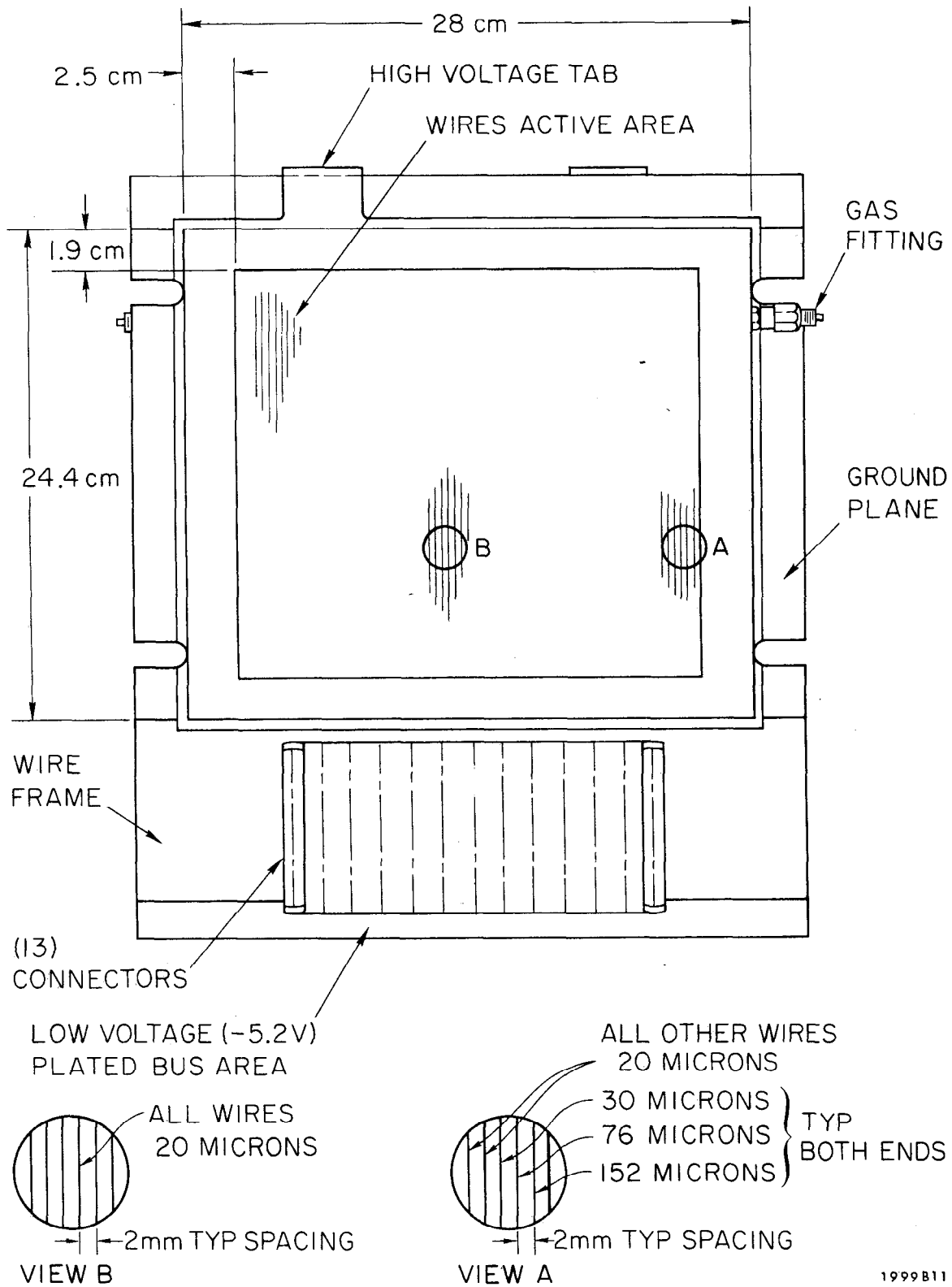
The Fraction of Events with Different Numbers of Tracks for a Typical Run

<u>Number of Tracks</u>		<u>Event Level</u>		
X	Y	1	2	3
0	0	0.0025 ± 0.0004	0.0006 ± 0.0006	0.01 ± 0.01
0	1	0.0016 ± 0.0003	0.010 ± 0.001	0 ± 0.01
0	2	0.0001 ± 0.0001	0 ± 0.0006	0 ± 0.01
0	3 or more	0 ± 0.0001	0 ± 0.0006	0 ± 0.01
1	0	0.0052 ± 0.0006	0.010 ± 0.001	0.02 ± 0.02
1	1	0.966 ± 0.002	0.948 ± 0.006	0.94 ± 0.02
1	2	0.0055 ± 0.0006	0.010 ± 0.001	0.02 ± 0.01
1	3 or more	0.0007 ± 0.0002	0.0006 ± 0.0006	0 ± 0.01
2	0	0.0003 ± 0.0002	0.0006 ± 0.0006	0 ± 0.01
2	1	0.012 ± 0.001	0.014 ± 0.003	0 ± 0.01
2	2	0.0039 ± 0.0005	0.004 ± 0.002	0.01 ± 0.01
2	3 or more	0.0005 ± 0.0003	0.0006 ± 0.0006	0 ± 0.01
3 or more	0	0 ± 0.0001	0 ± 0.0006	0 ± 0.01
3 or more	1	0.0010 ± 0.0002	0.0012 ± 0.0008	0 ± 0.01
3 or more	2	0.0006 ± 0.0002	0.0006 ± 0.0006	0 ± 0.01
3 or more	3 or more	0.0002 ± 0.0001	0 ± 0.0006	0 ± 0.01

FIGURE CAPTIONS

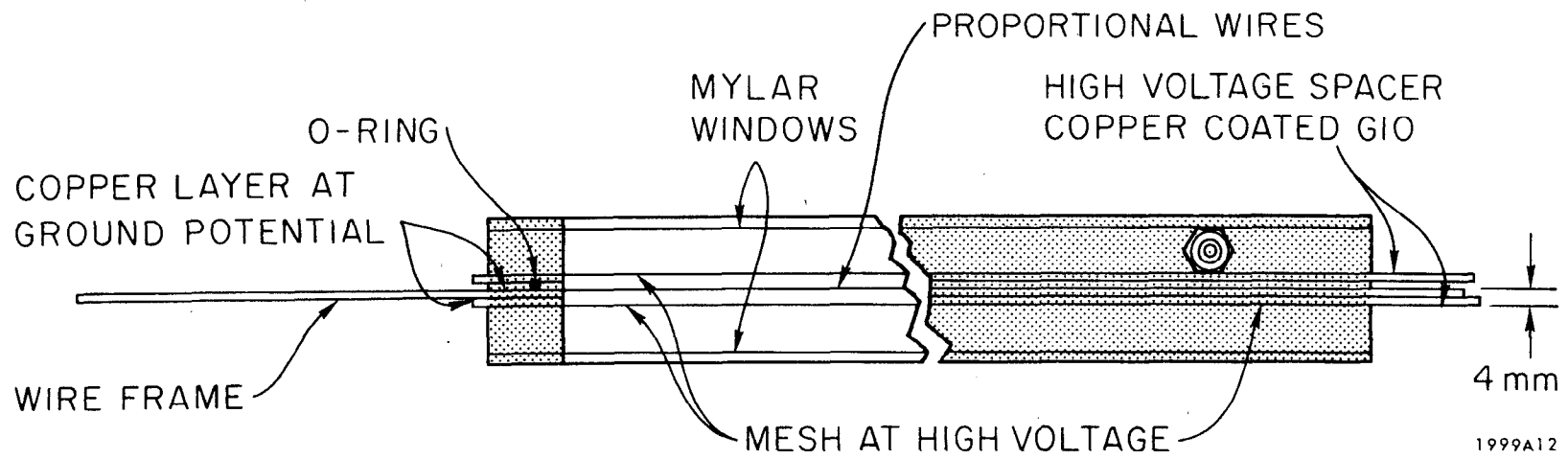
1. (a) Top view of a proportional chamber with details of the wires near the edge of and at the center of the active area.
(b) Cross section view of a proportional chamber. Note the 4 mm high voltage to proportional wire spacing.
(c) Detail of the wire frame showing the traces leading from the proportional wires to the connector. Each wire is isolated from its nearest neighbor by a pin connected to ground.
(d) Photograph of one of the proportional wires taken with 1100 times magnification.
2. The delay curve for a chamber in a test beam. The efficiency of the chamber as a function of the delay in the gate signal.
3. Photograph of the two halves of a proportional chamber with mounting frame.
4. Photograph of an assembled proportional chamber.
5. Block diagram of the electronics for a single wire.
6. Amplifier circuit diagram with typical pulse shapes for minimum ionizing particles.
7. Photograph of the amplifier card. The isolation between wires established on the wire frame is continued on the amplifier card.
8. Circuit diagram of a single latch channel.
9. The detector scheme of the 20-GeV spectrometer.
10. Photograph of the detector of the 20-GeV spectrometer. The scintillation counter and proportional chamber in the foreground are TR1 and Y1, respectively.
11. The delay curve for chamber Y2. The inefficiency ($=1 - \text{efficiency}$) as function of the delay in the gate signal.

12. The probability that an event will have N wires in chamber Y2 for a typical run. The other chambers had similar performance.
13. (a) The probability a run had a fraction F of events with one group in each X chamber. The distribution is separately normalized for each event level.
(b) The probability a run had a fraction F of events with one group in each Y chamber.
14. The probability a run had a fraction F of events with one track in both the horizontal and vertical. The distribution is separately normalized for each event level.
15. (a) The distribution of events in chamber Y2 summed over several runs. The arrows indicate the limits of the fit discussed in the text.
(b) The deviations of counts in chamber Y2 from a linear fit. The indicated error includes the statistical error and the random variation in the bin-to-bin efficiency.



1999B11

Fig. 1A



1999A12

Fig. 1B

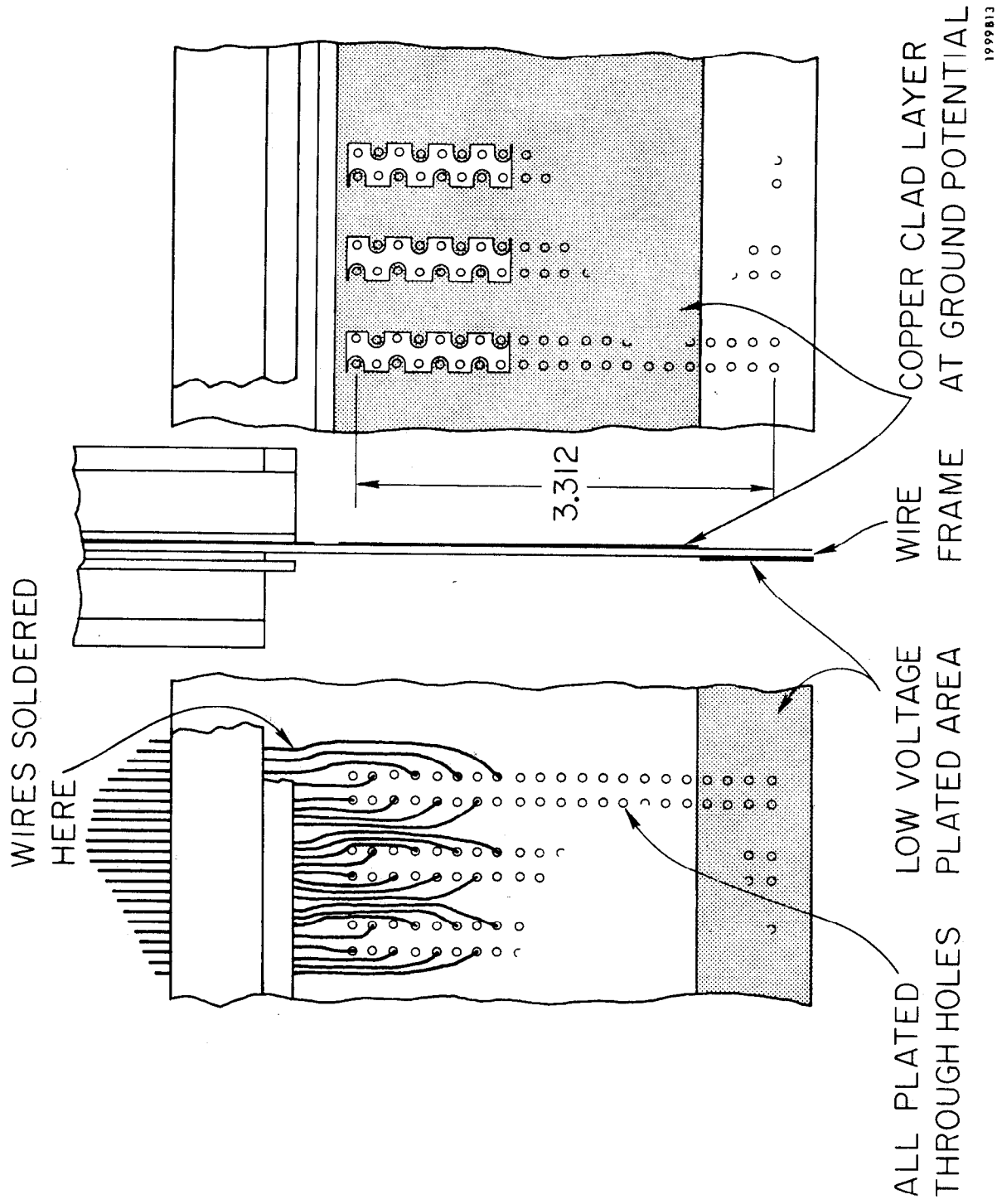
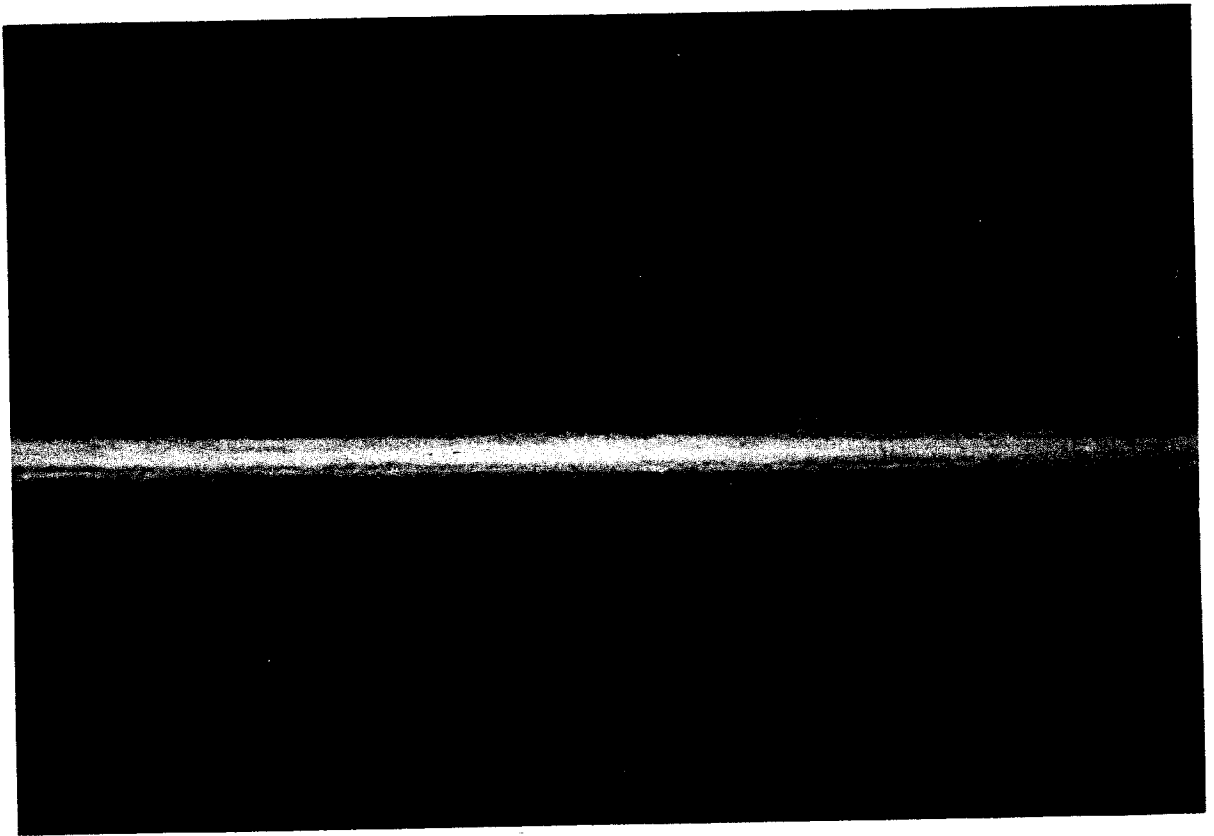
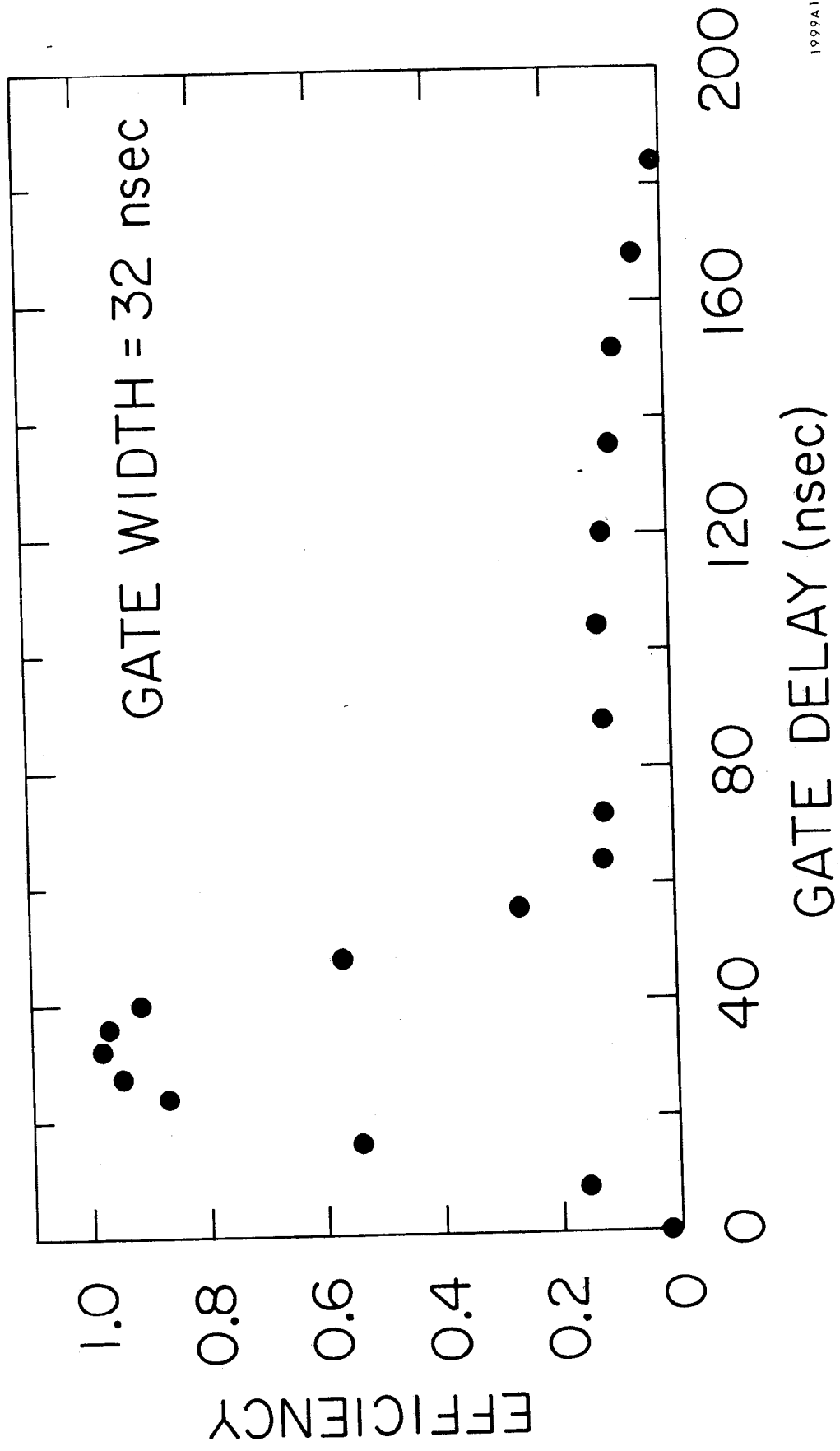


Fig. 1c



1999A14

Fig. 1D



1999A1

Fig. 2

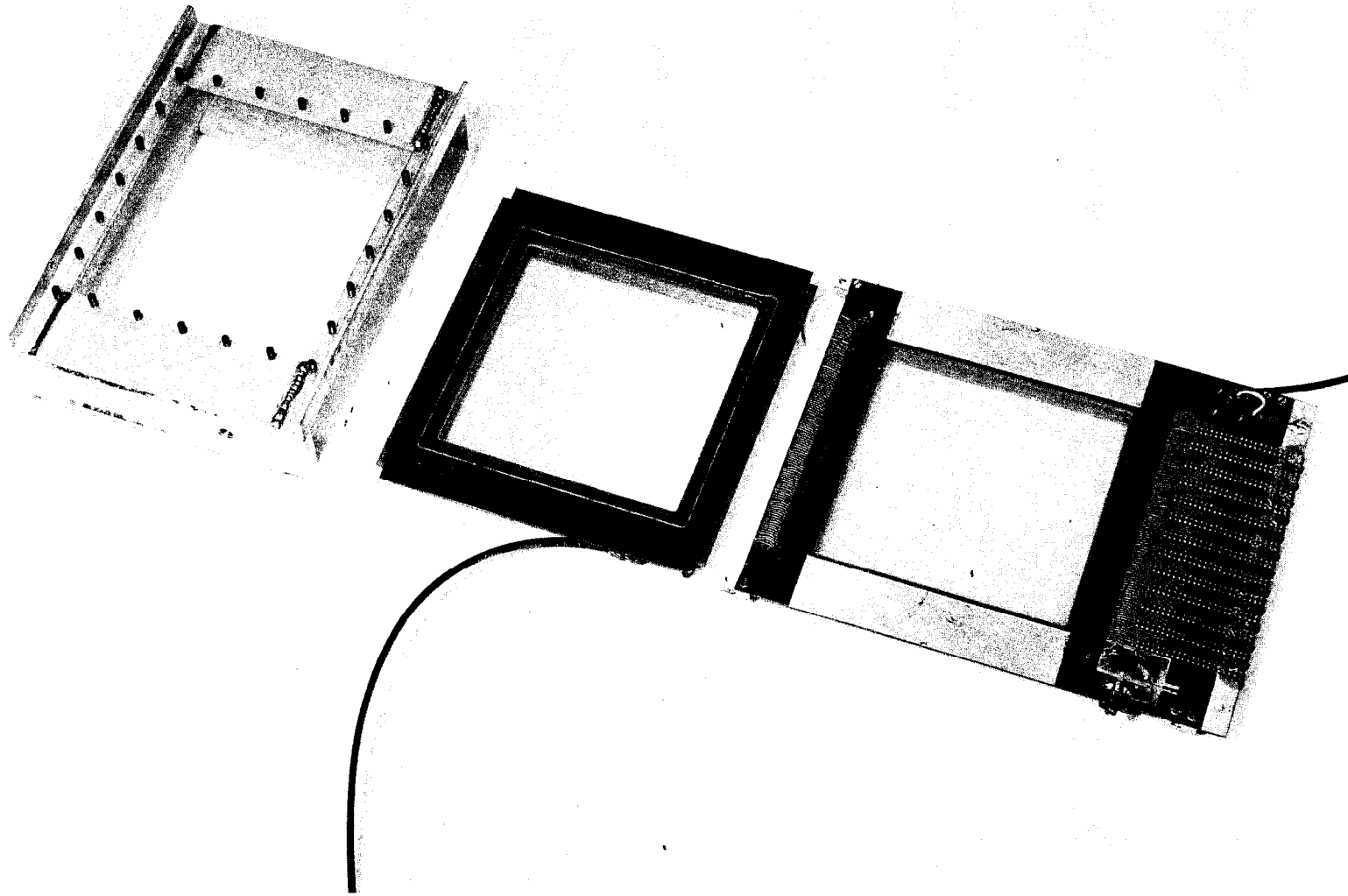
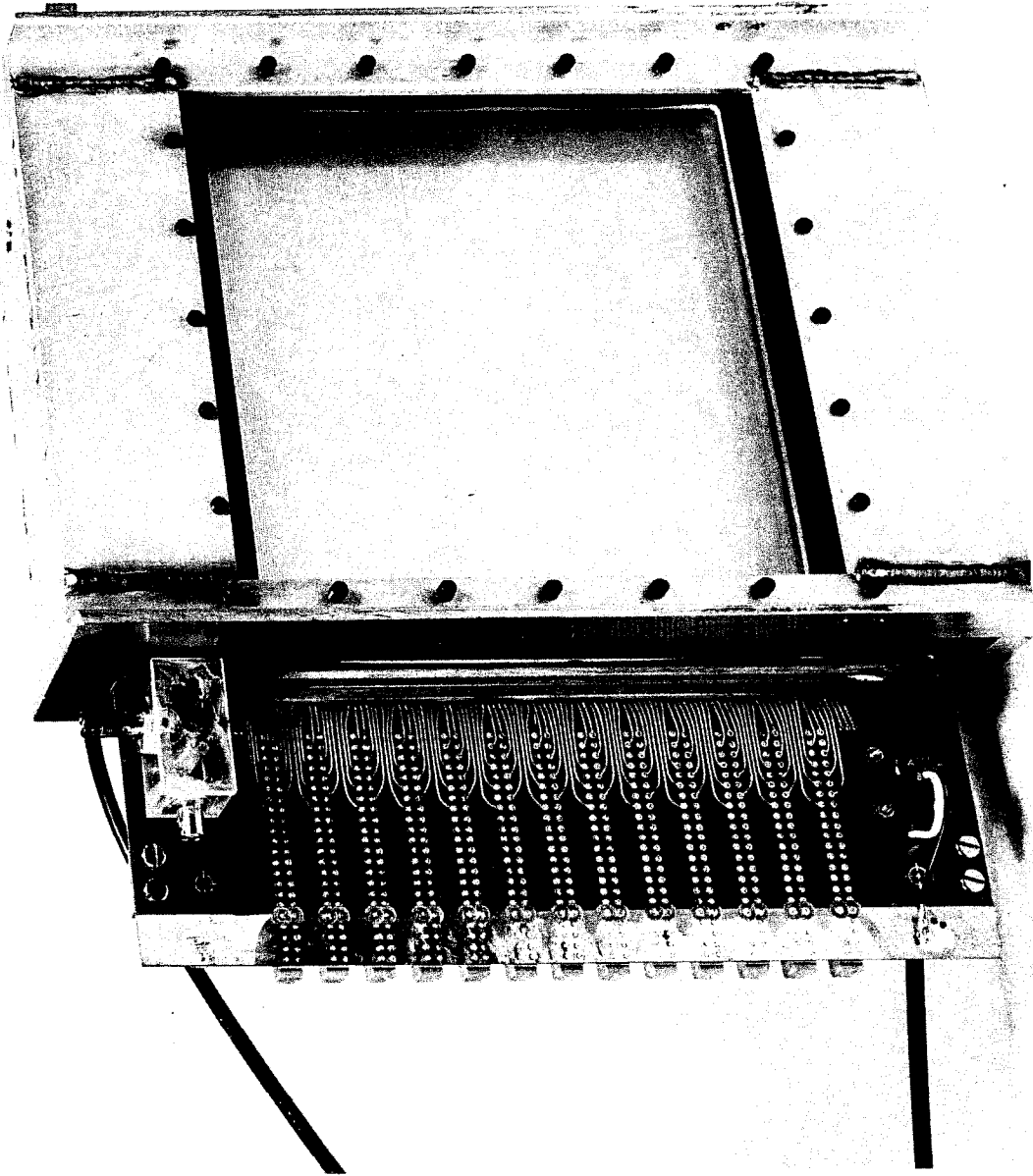


Fig. 3

1999A20

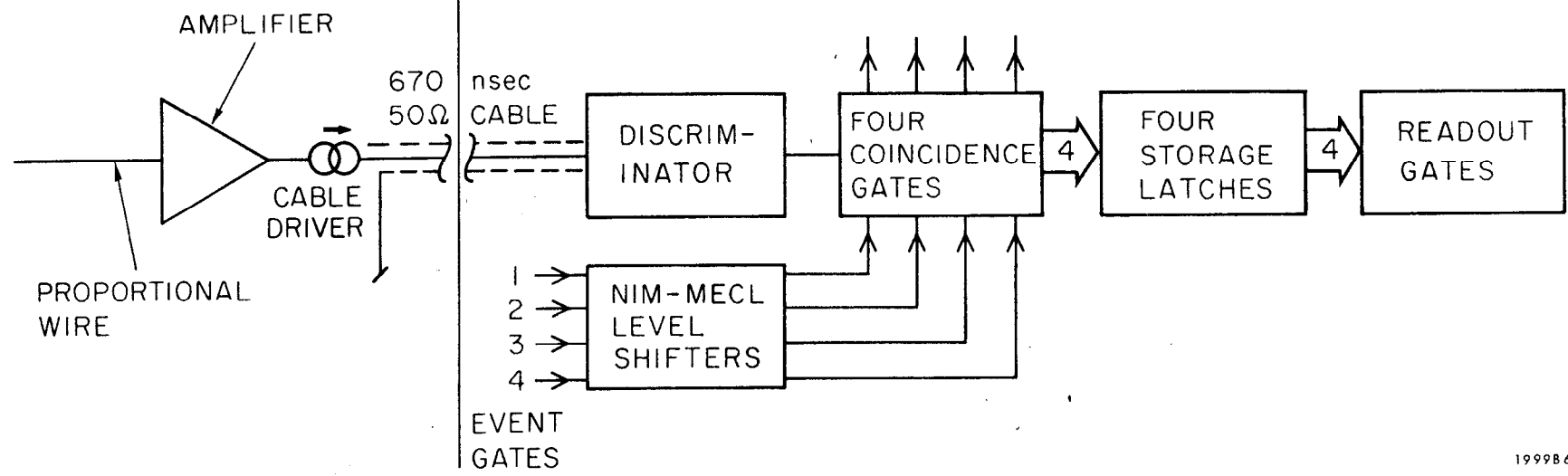


1999A19

Fig. 4

20 GeV SPECTROMETER

COUNTING HOUSE



199986

Fig. 5

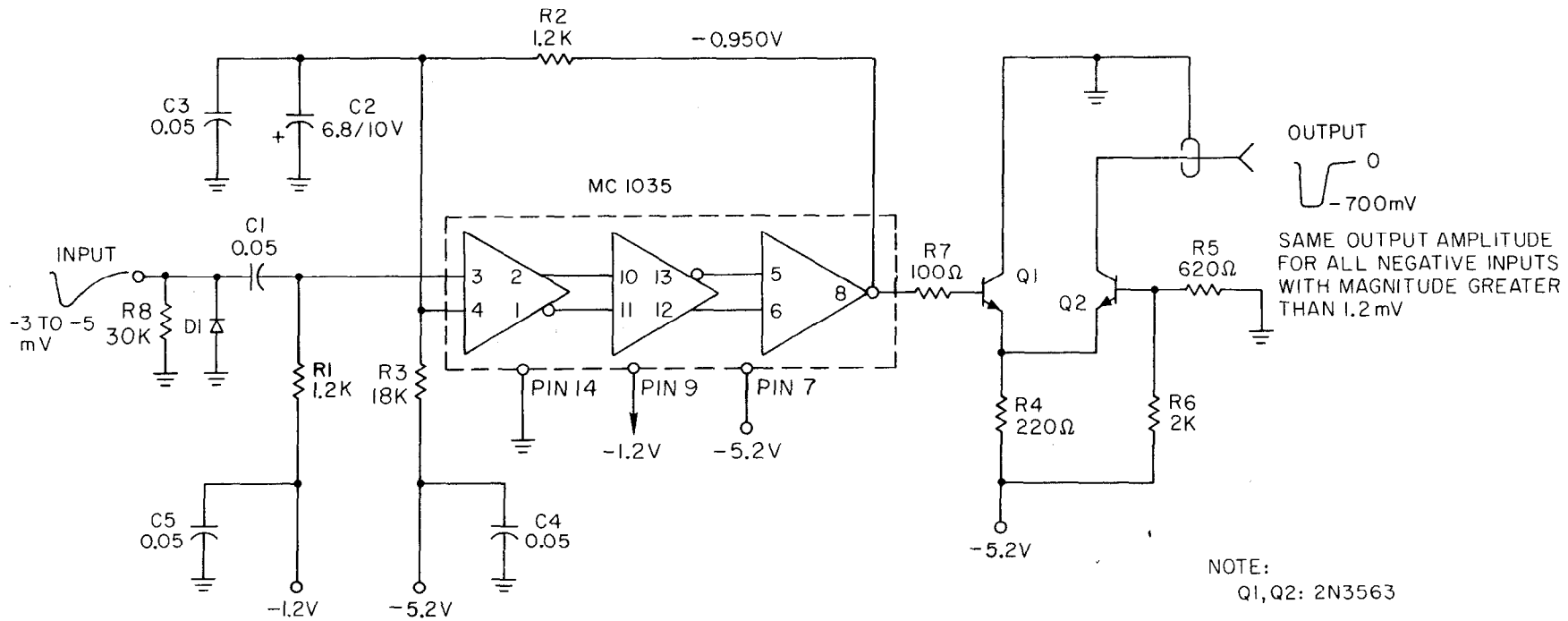
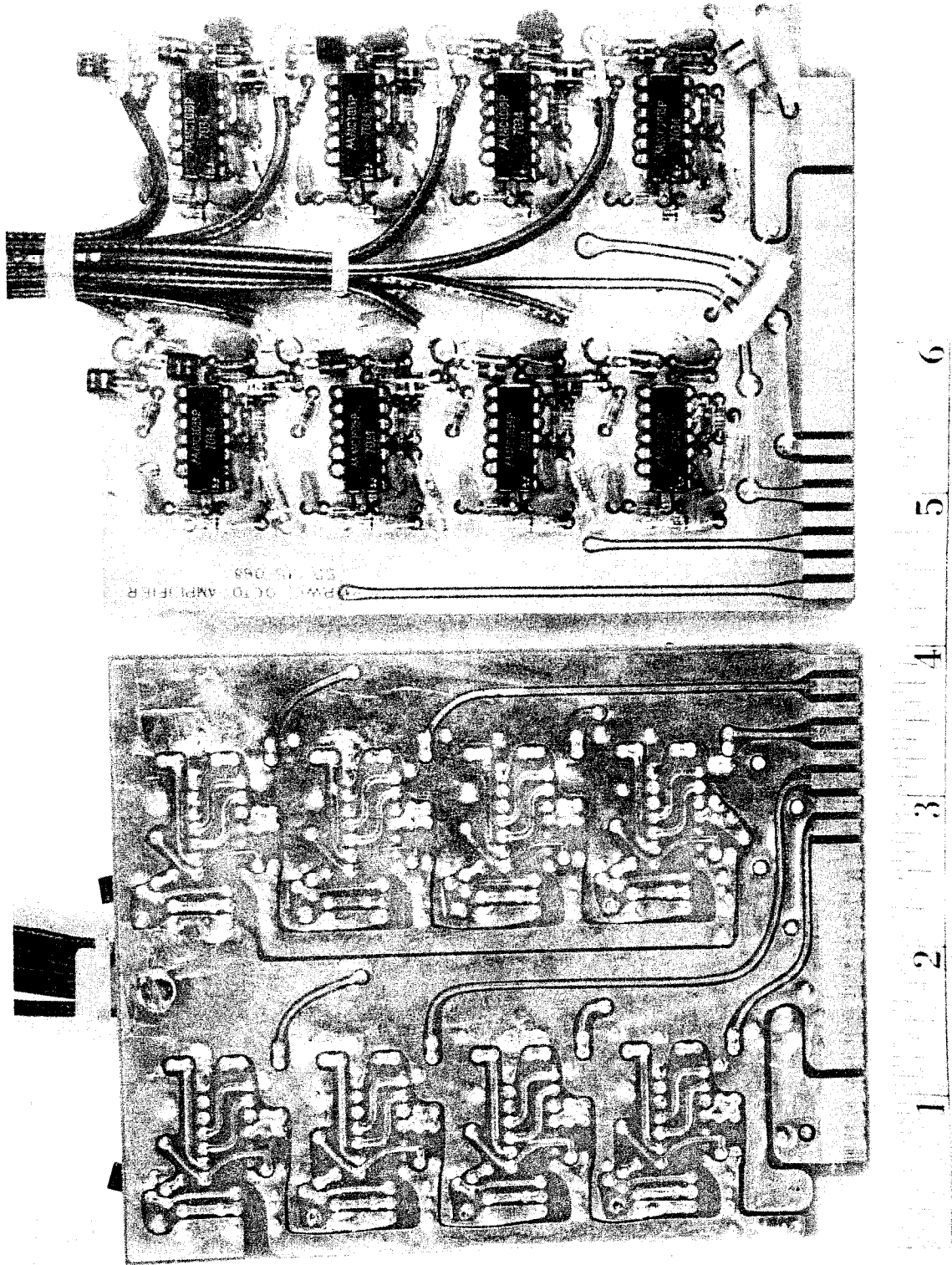
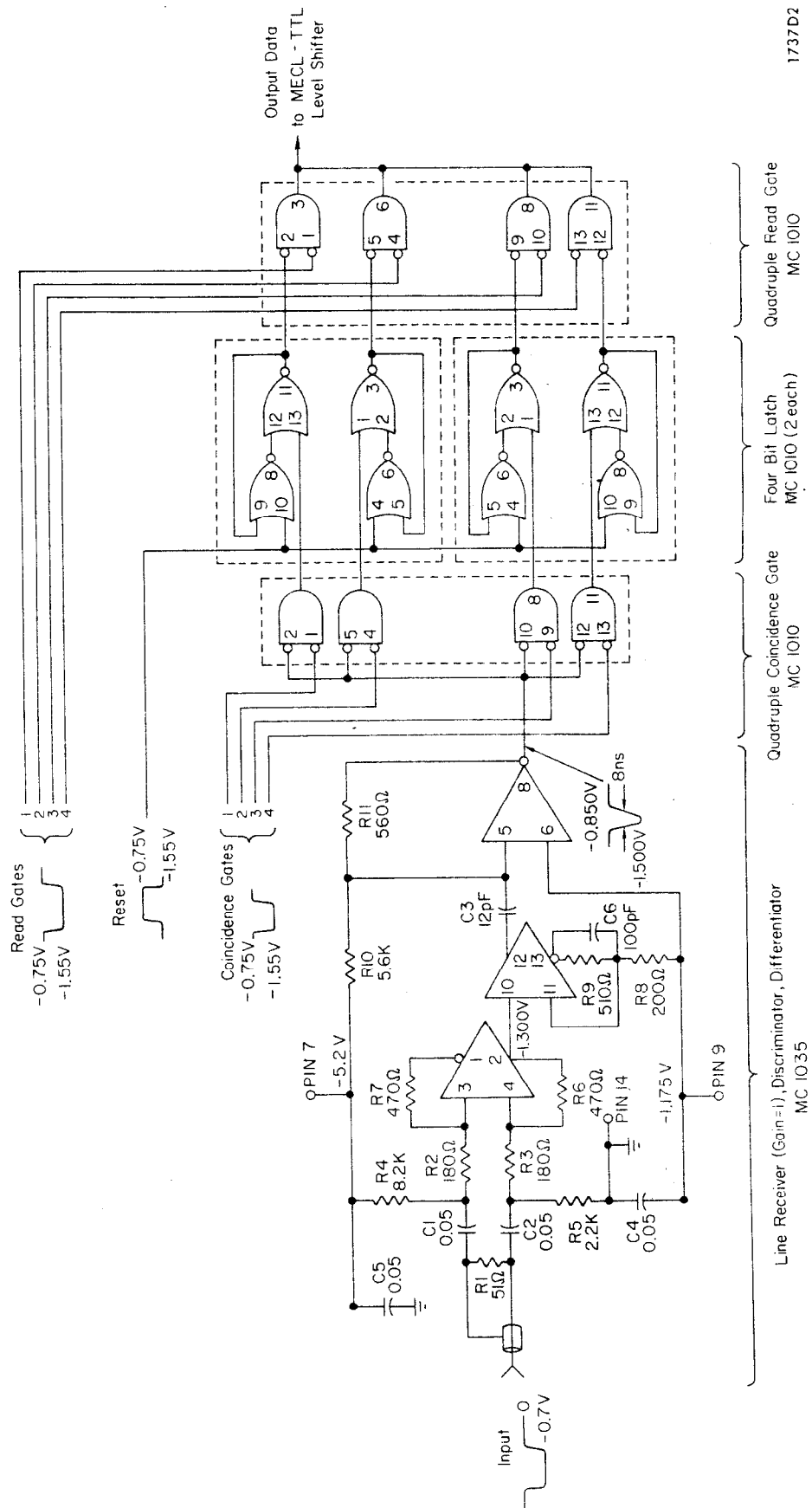


Fig. 6



1737A13

Fig. 7





1737D2

Fig. 8

DISTANCES IN cm

PARTICLE DIRECTION 

 SCINTILLATION COUNTER
 PROPORTIONAL CHAMBER

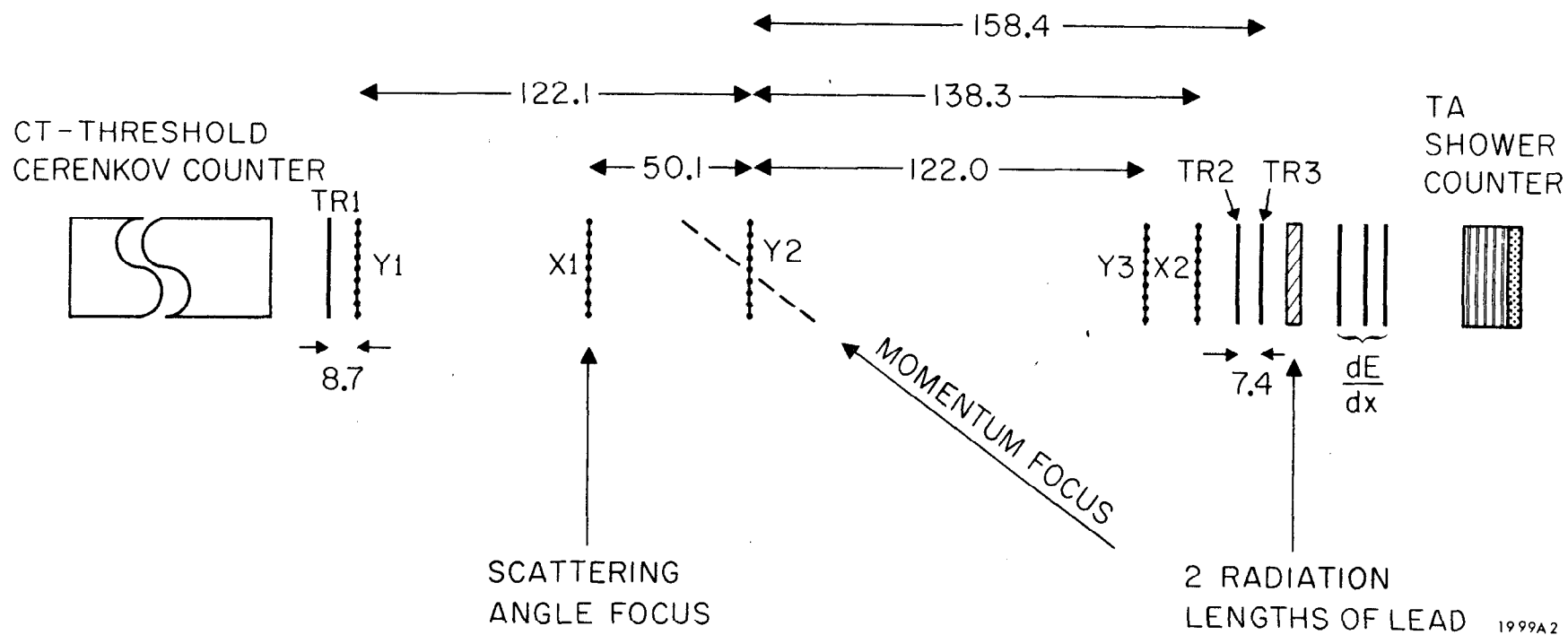
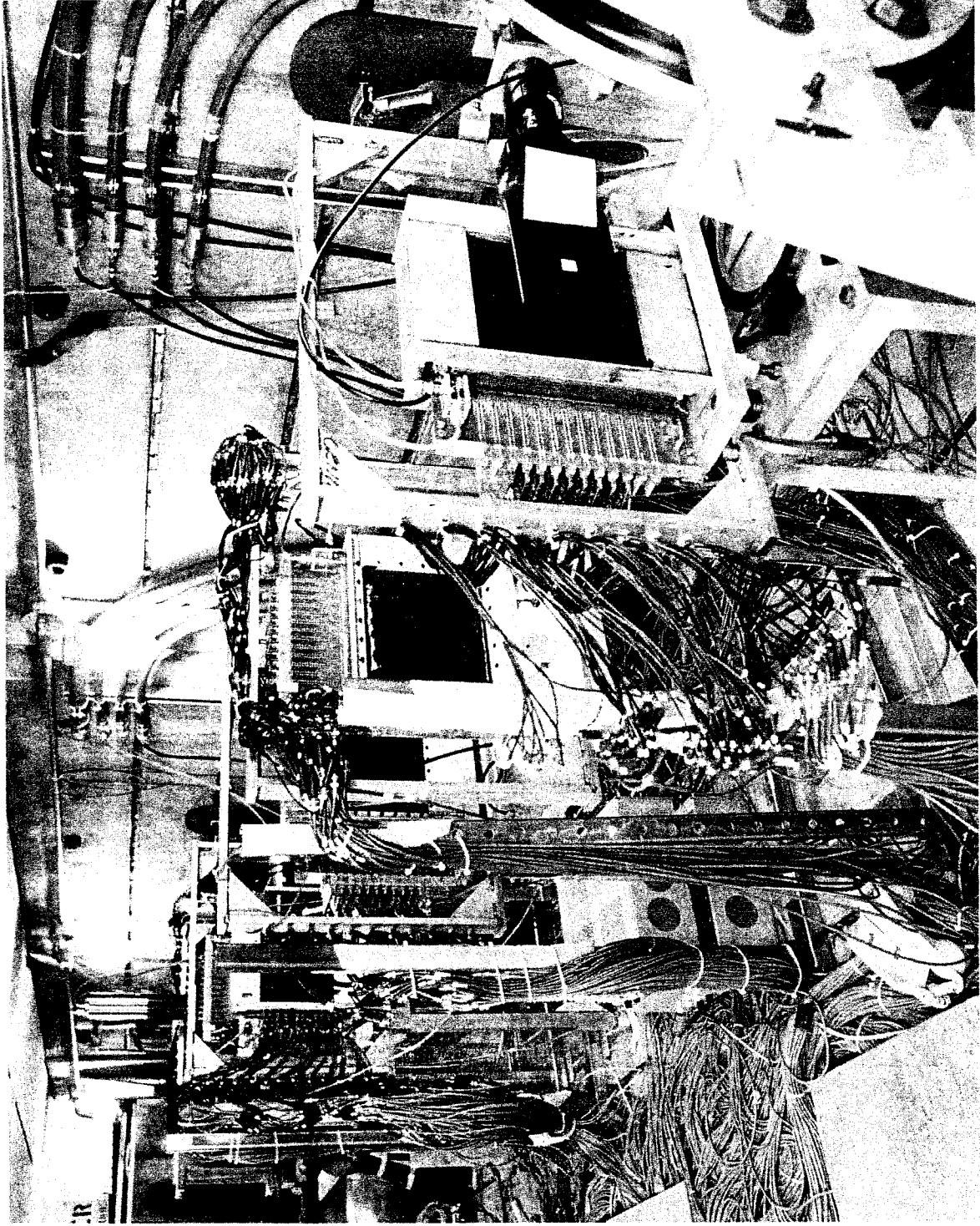


Fig. 9



1999A18

Fig. 10

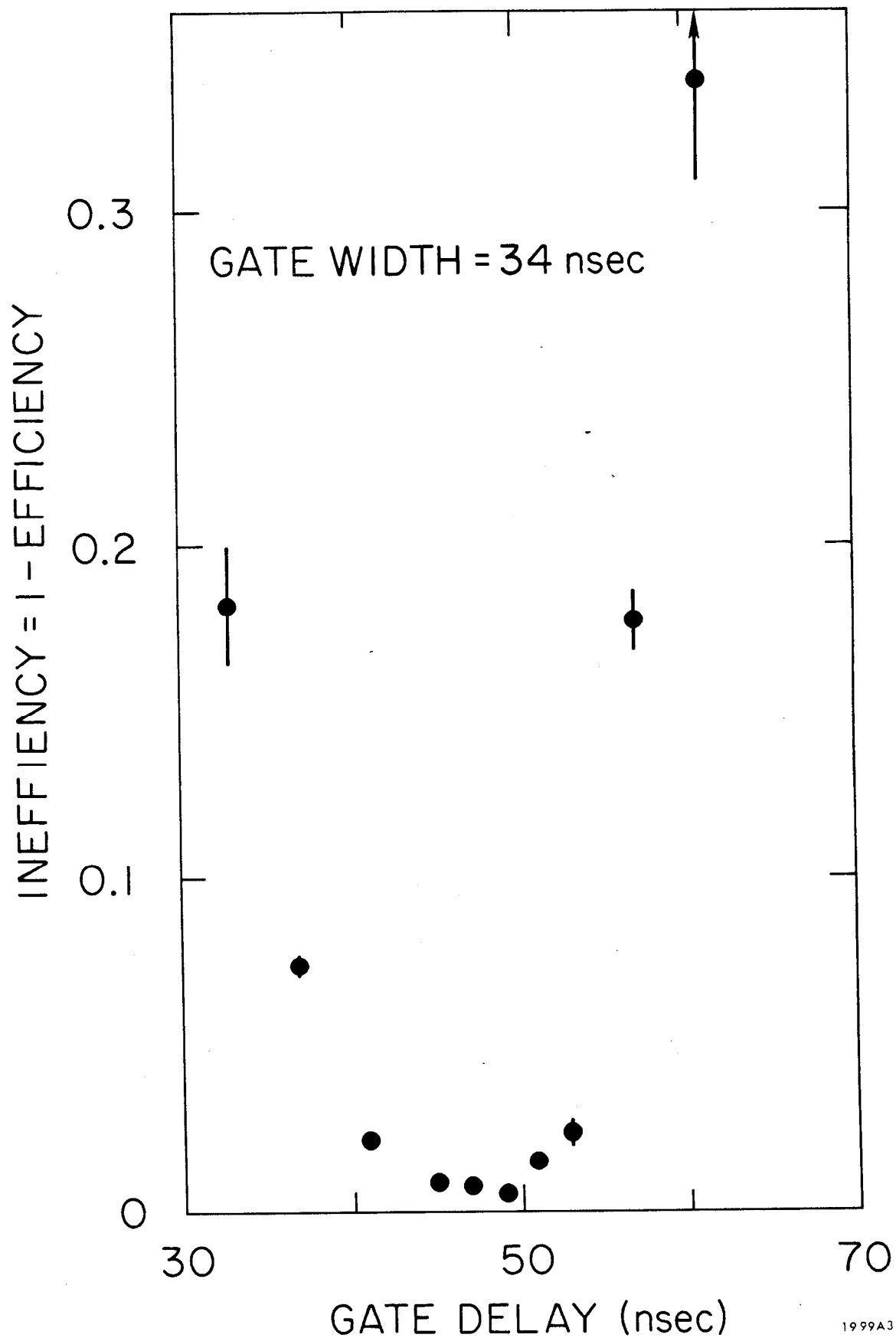


Fig. 11

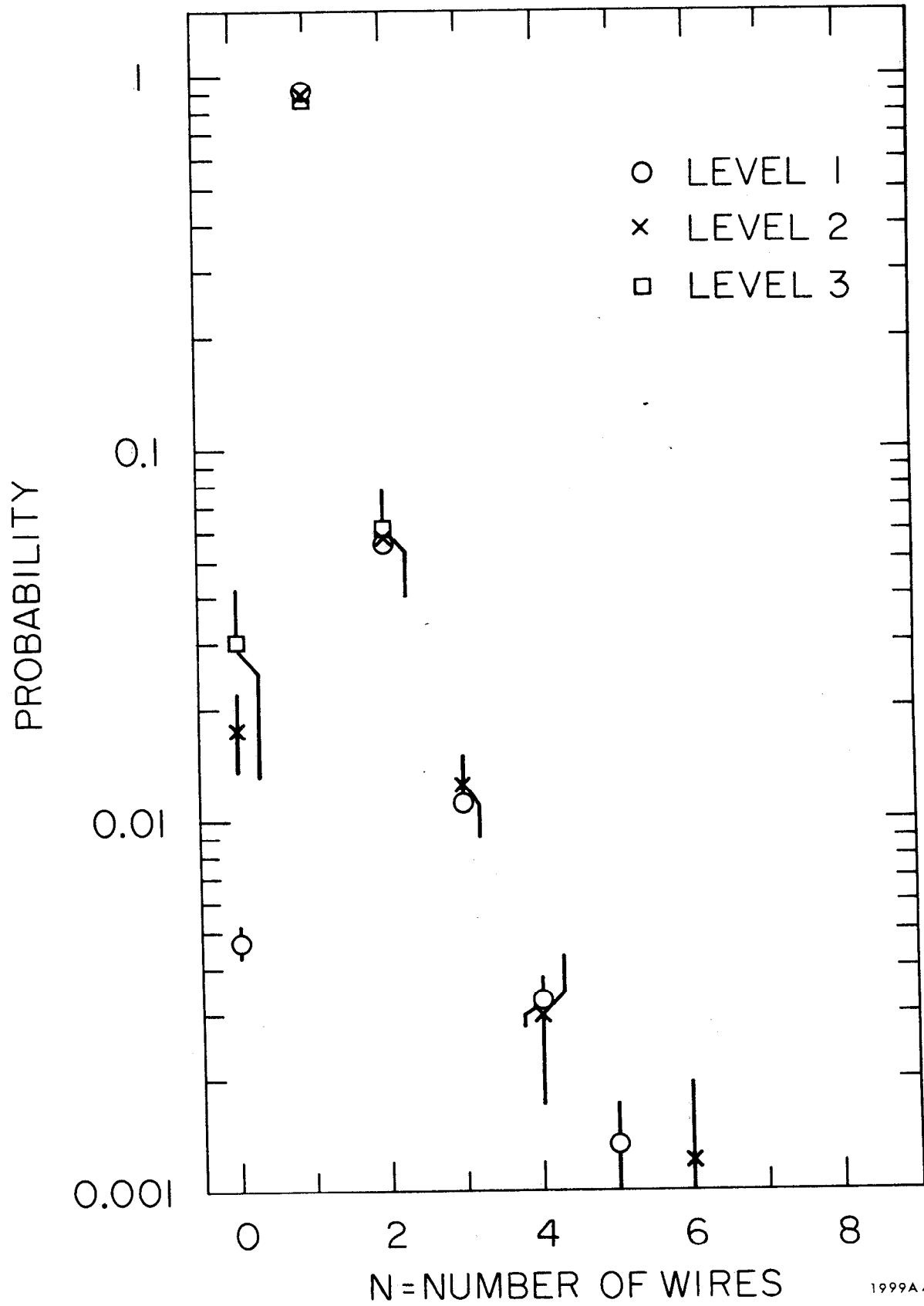


Fig. 12

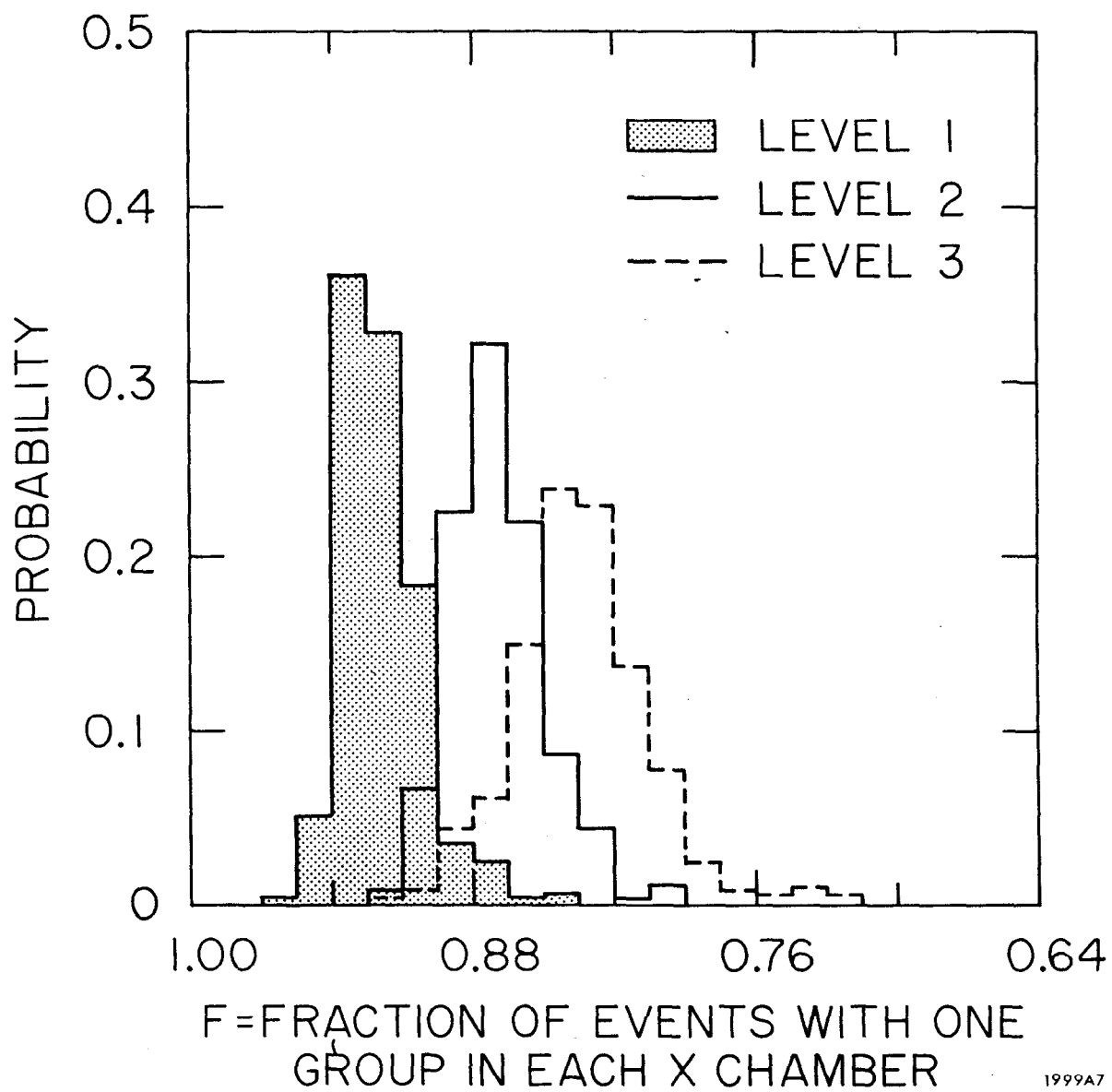


Fig. 13A

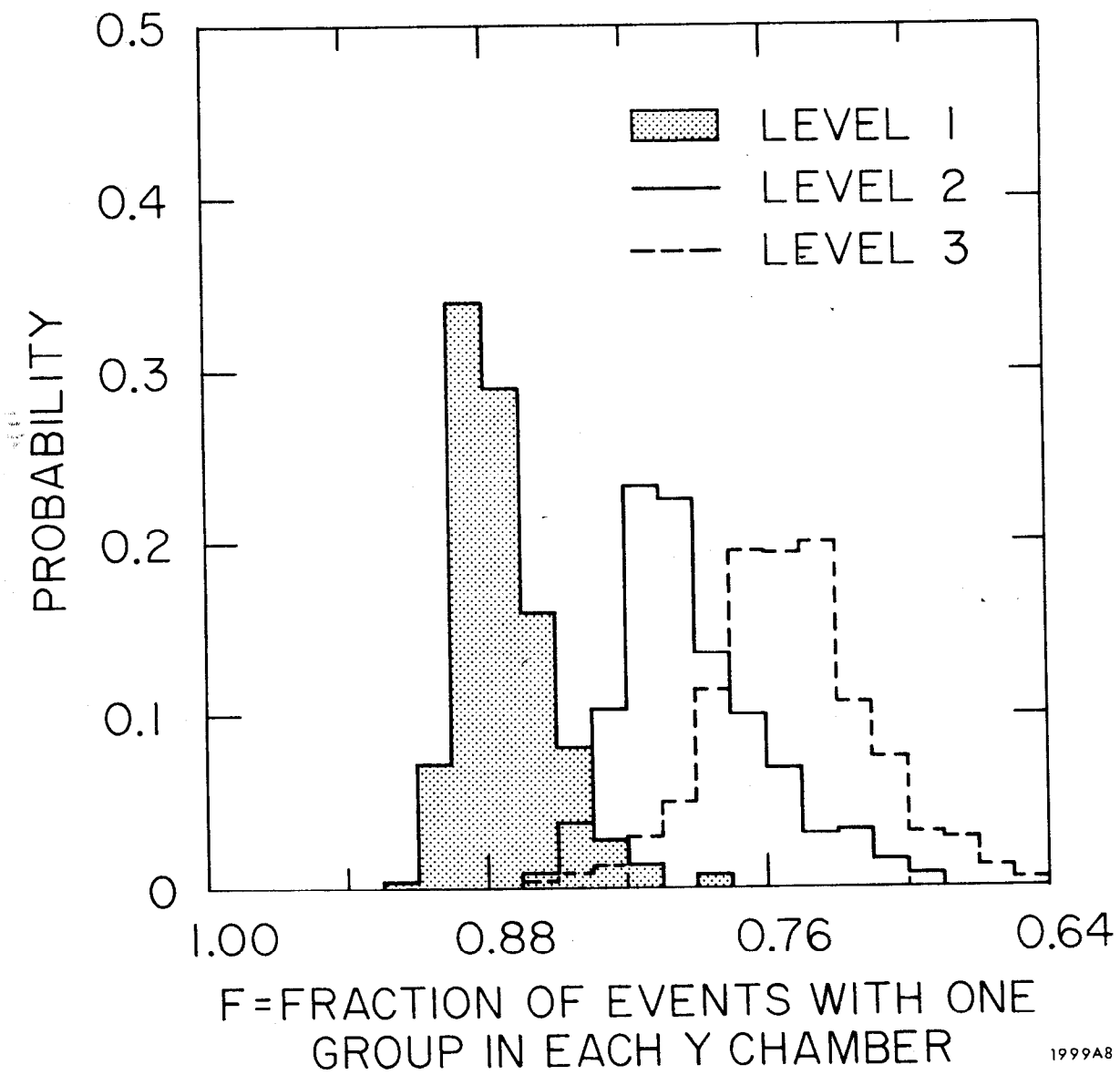


Fig. 13B

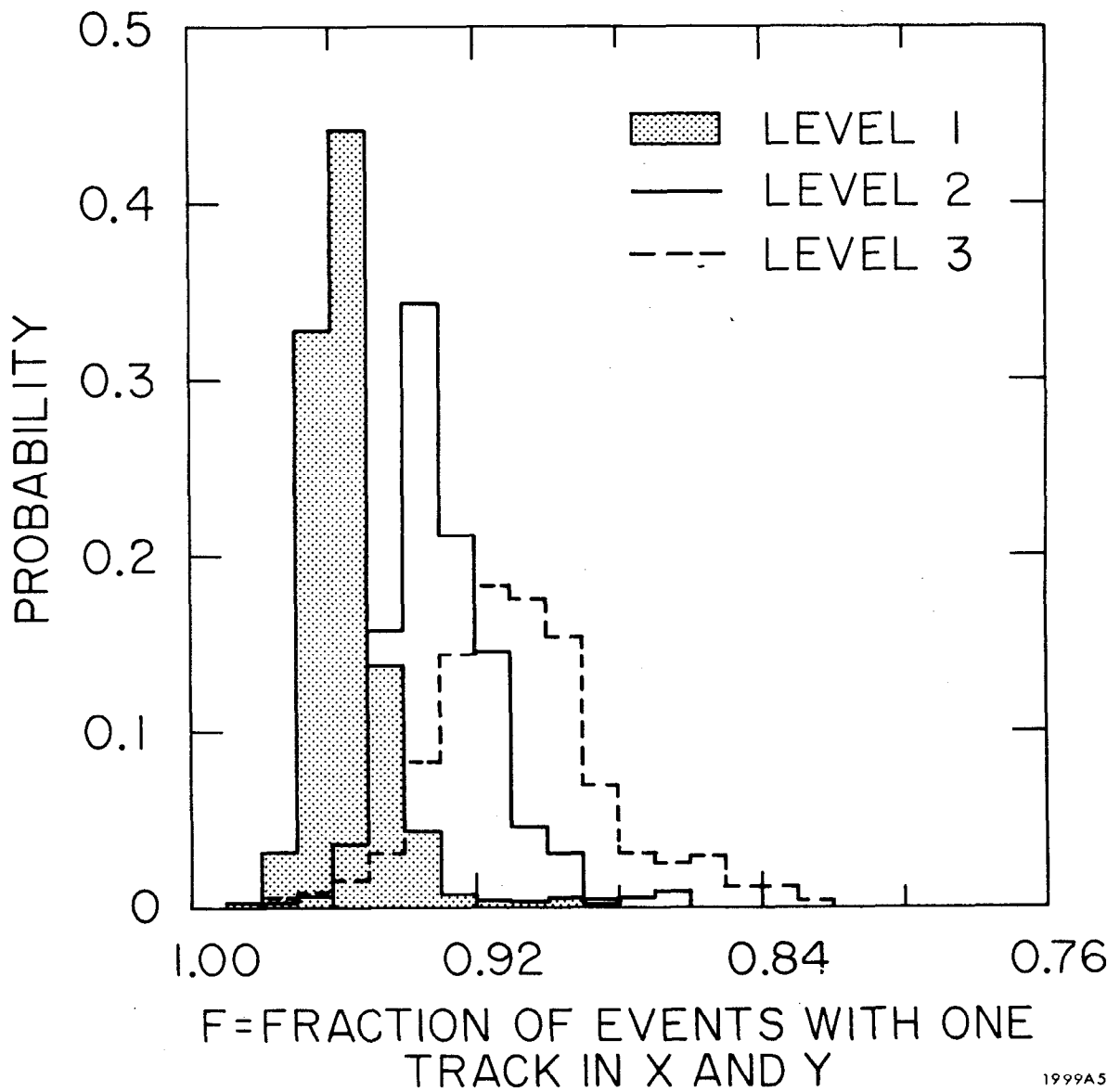


Fig. 14

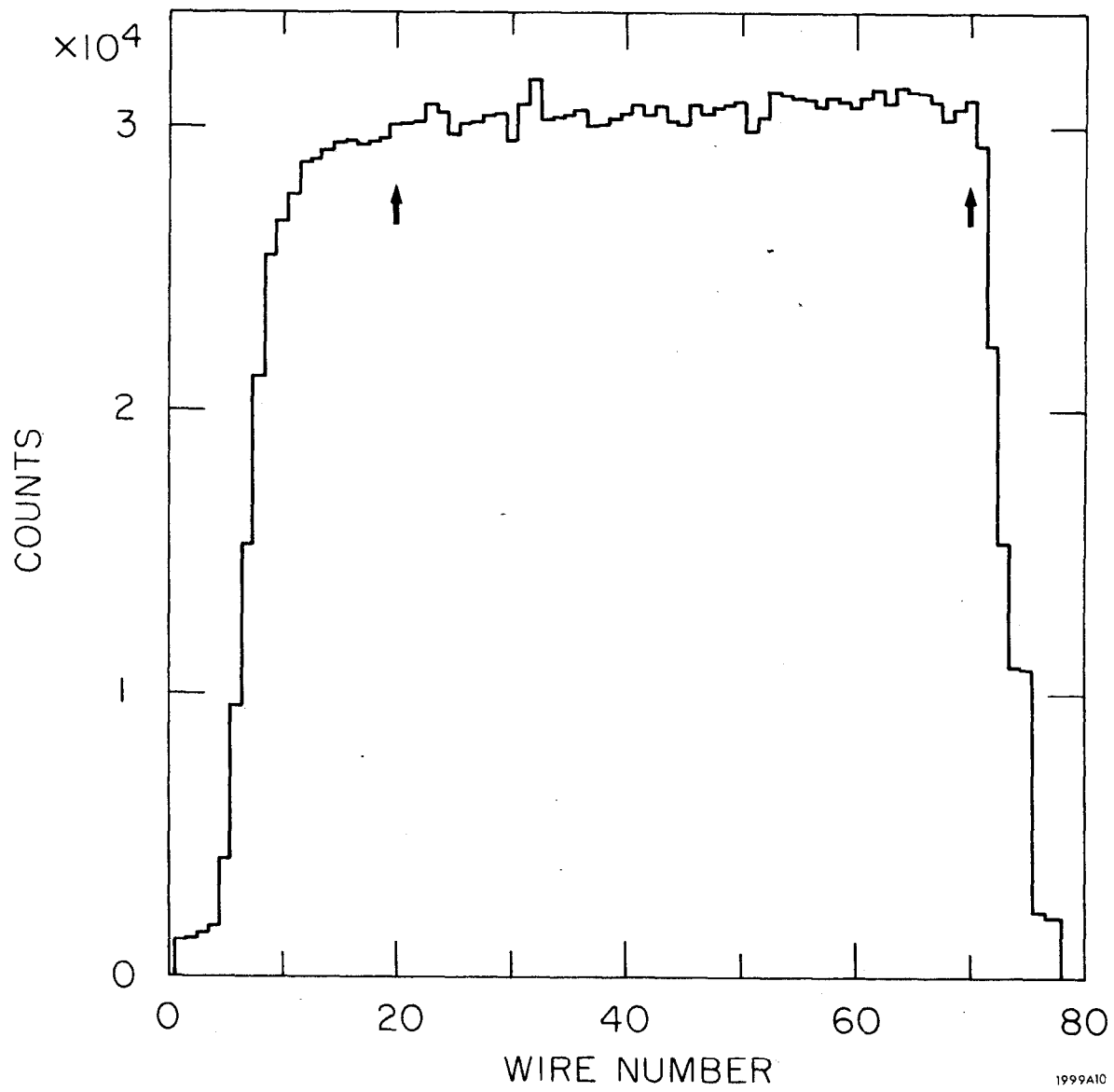
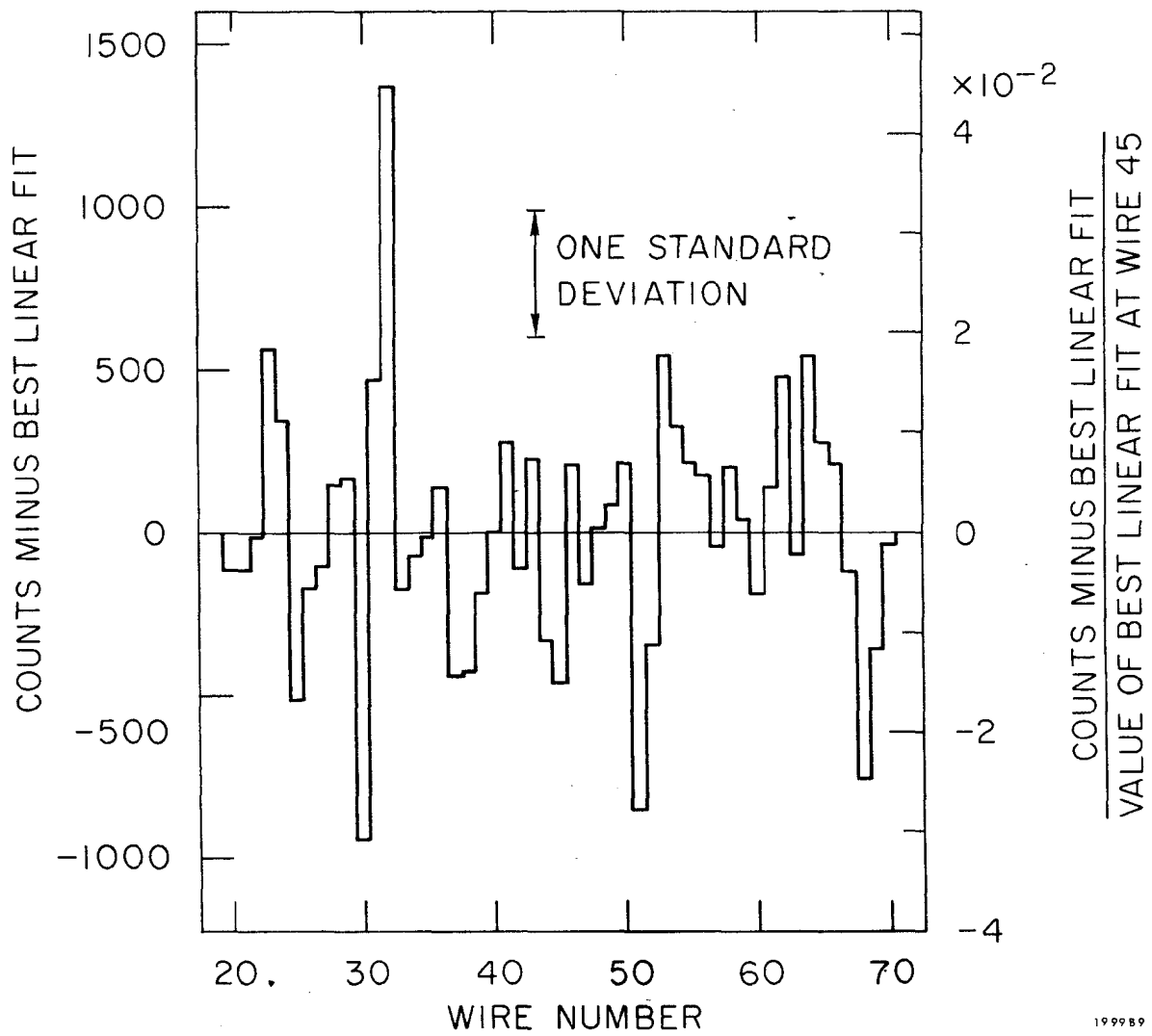


Fig. 15A



1999B9

Fig. 15B